Synchrony dynamics of dissolved organic carbon in high-mountain streams: insights into scale-dependent processes

Lluís Gómez-Gener[1,2*], Nicola Deluigi[1], Tom Battin[1]

[1] River Ecosystems Research Laboratory, Alpine and Polar Environmental Research Center (ALPOLE), Ecole Polytechnique Fédérale de Lausanne, EPFL, Switzerland

[2] Centre for Research on Ecology and Forestry Applications, Universitat Autònoma de Barcelona, Campus de Bellaterra, Edifici C, 08193 Cerdanyola del Vallès, Barcelona, Spain

* E-mail: gomez.gener87@gmail.com (Corresponding author)

Running head: High-mountain stream DOC synchrony dynamics

Abstract

In high-mountain landscapes, biological resources such as organic carbon (OC) are often limited and heterogeneously stored in poorly developed soils, snow, ground ice and glaciers. Climate change influences the dynamics of OC mobilization to- and processing into- the recipient streams. These patterns can vary from seasonal (e.g., snow melt in spring) to daily (e.g., ice melt in summer) depending on the location of the streams within the catchment. Capturing the temporal richness of stream biogeochemical signals is now a reality with the advent of high-resolution sensors. In this study, we used wavelet analysis on high-frequency discharge (Q) and dissolved organic carbon (DOC) measurements from nine streams in the Swiss Alps to investigate whether synchrony (S) of Q (S_Q) and DOC (S_{DOC}) persisted or collapsed among streams, and its response to spatial position, climate and land cover gradients across different time scales. Our findings reveal that short-term (0-10 days) S_Q and S_{DOC} were strongly influenced by distance between streams and network connectivity. In contrast, catchment-related properties (i.e., altitude or land cover) were more important in driving S_Q and S_{DOC} dynamics at longer time scales (>50 days). However, the degree to which local catchment properties controlled S patterns at the longest timescales depended both on the response variable (i.e., Q vs. DOC) as well on the main land cover (i.e., vegetation vs. glacier). Elucidating most prominent timescales of S_{DOC} is relevant given the hydrological alterations projected for high-mountain regions. We show that glaciers impose a unique seasonal regime on DOC concentration, potentially overriding the effects of other local hydrological or biogeochemical processes during downstream transport. Consequently, S_{DOC} dynamics in high-mountain streams may change as glaciers shrink, thereby altering downstream opportunities for biogeochemical transformations.

Introduction

Predicting how spatial and temporal variability changes with scale of observation is one of the fundamental interests of both landscape ecology (Turner et al. 1989; Levin 1992) and catchment hydro-biogeochemistry (McGuire et al. 2014). Part of this impetus is the recognition that many environmental processes are regional, continental or even global in nature (Turner et al. 1989). However, our ability to scale up process dynamics from single sites to broader areas is still limited.

Ecosystem dynamics result from both extrinsic and intrinsic controls. In freshwater ecosystems, extrinsic controls are predominantly linked to climatic factors, such as air temperature, precipitation, solar radiation or wind, and they exert a rather uniform influence over large regions (Magnuson et al. 1990). Accordingly, to the extent that spatially separated ecosystems (or their properties) within a region behave similarly over time (i.e., spatial synchrony or temporal coherence, *sensu* Magnuson et al., 1990), it becomes easier to make generalizations about how they will respond to climate variations. Therefore, freshwater ecosystems within a certain region are expected to respond similarly to climatic events, such as a multi-year drought, a series of cool, wet years, or systematic year-to-year variations (Kratz et al. 1998). However, a series of pioneering multi-lake studies (Magnuson et al. 1990; Kratz et al. 1998; Soranno 1999; Baines et al. 2000) have also shown that synchrony between lakes depends on both the nature of the variable under study (e.g., physical, chemical, and biological properties) and the sensitivity of such variables to intrinsic controls such as local characteristics or internal lake dynamics (e.g., lake shape or basin characteristics). For example, some physical variables, such as surface temperature and ice-out date, exhibit strong synchrony over distances greater than 1000 km (Wynne et al. 1996; Kratz et al. 1998). On the other hand, some biological and chemical variables (e.g., algal biomass or nutrients) are less synchronous than most physical variables and semi-conservative chemical species (Magnuson et al. 1990; Kratz et al. 1998). Consequently, by examining patterns of temporal coherence, we can identify the spatial extent to which dynamics within aquatic ecosystems change or collapse in response to climatic change versus local processes (i.e., the degree of regional generalizations for effects of climate change). In other words, temporal coherence indicates the extent to which observed responses may be extrapolated to the broader landscape (Magnuson et al., 1990).

In contrast to lake ecosystems, rivers are relatively open ecosystems that form networks spanning multiple catchments and are inherently connected to landscapes through matter exchange (Hynes 1975; Vannote et al. 1980; Frissell et al. 1986; Fisher et al. 1998). As a consequence, the transferability of lake-based models might not be straightforward for understanding the synchrony dynamics between stream pairs within fluvial networks (e.g., Seybold et al., 2021). Instead, accounting for other filters such as landscape position, land-stream interaction or network connectivity might be necessary to better understand the synchronous versus asynchronous responses of streams to climate variability. To overcome this issue, we propose adapting the landscape position concept from lake districts (e.g., *sensu* Webster et al. 1996; Baines et al. 2000) to fluvial networks and exploring its applicability for the analysis of synchrony dynamics between contrasted variables in both connected or disconnected streams within the same region. Climate signals are filtered (i.e., attenuated and/or scattered) by both landscapes and riverscapes to reduce the synchrony between stream pairs or create nonlinear responses of synchrony across distance gradients (Figure 1a). The dynamics of any dissolved constituent in a stream are largely determined by both land cover and its connectivity with upstream waters and lateral catchment sources (Hynes 1975). Based on this, a pair of stream segments draining catchments with different landscape compositions and/or not connected through the river network (A-B pair in Figure 1a) will be less synchronized for a specific dissolved constituent in stream water, regardless their lineal geographical distance, compared to a pair of streams with similar land cover proportions or sharing the same network branch (A-C in Figure 1a). As an example, forested and non-forested catchments not only differ in how dissolved constituents are spatially created and stored but also, because this heterogeneity includes differences in their vertical profiles, in how they are mobilized into streams in response to changes in flow (Tank et al. 2018; Gómez-Gener et al. 2021).

In addition to the spatial dimension, timescale-dependent controls on aquatic ecosystem processes have been identified in numerous long-term time series (Likens 1989; Hampton et al. 2019; Wilkinson et al. 2020). This includes the effect of processes operating within fractions of seconds (biochemical reactions), from seconds to days (non-biological processes such as rain events/hydrological pulses), and from days to weeks or even months (snowmelt events, solar cycles). Because the mechanism driving synchrony of a certain water constituent may operate at specific timescales (Defriez et al. 2016, 2017; Sheppard et al. 2016; Walter et al. 2017; Anderson et al. 2019), synchrony will manifest itself differently across timescales (Figure 1b). Nevertheless, the complexity of high-frequency signals challenges our ability to identify synchronies (or asynchronies) between stream locations and/or variables of interest because (1) traditional monitoring, normally based on weekly or monthly grab measurements (Kirchner et al. 2004; see examples above), fails in capturing some of these responses (e.g., short-term events driven by rapid changes in water flow paths), and (2) standard approaches for assessing synchrony (i.e., correlation analysis) assume linearity and uniformity across timescales. With the advent of affordable and reliable sensor technology, high-resolution measurements across a broad range of solutes over prolonged periods are possible (Rode et al. 2016; Marcé et al. 2016). This enables an increase in the temporal richness of signals and, more importantly, the capture of processes dynamics occurring at high frequencies. Additionally, novel approaches have enabled the isolation of complex patterns into those timescales of variability with the most interest and/or significance (i.e., wavelet coherence; Torrence and Compo 1998; Grinsted et al. 2004; Cazelles et al. 2008).

Here we take advantage of these advances to improve the understanding of the patterns and processes regulating the transport and cycling of solutes in heterogeneous headwater landscapes spanning a high diversity of temporal signals. To do so, we applied synchrony (S) analysis to three years of high frequency measurements (every 10 minutes) of discharge and dissolved organic carbon (DOC) from nine high-mountain stream segments distributed over three catchments in the Western Swiss Alps. With this approach, S patterns can reveal whether similarities between stream pair dynamics are more persistent across temporal scales or, in contrast, frequency-dependent non-linearities arise in cases of lower pair similarity. Identifying groups of streams that respond similarly to hydro-climatic fluctuations will enhance our ability to monitor the effects of climate variability and land cover change in high-mountain regions, choose appropriate reference ecosystems, and detect local deviations from the regional norm. This has become a remarkable task given the profound climate-driven hydrological and physicochemical changes that these streams are facing.

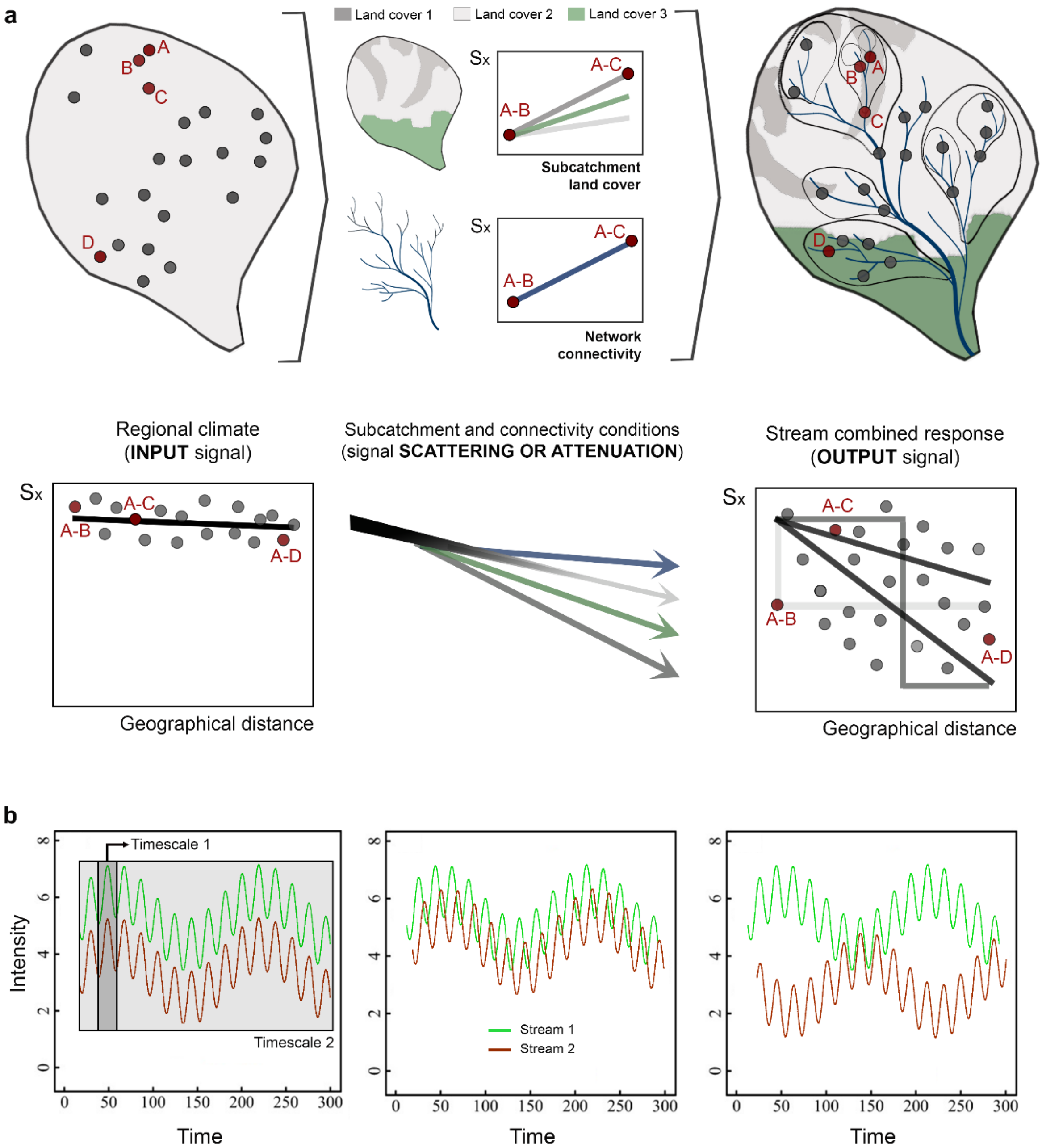

Figure 1. Conceptual figure illustrating both the spatial (**a**) and temporal (**b**) structure of solute synchrony between streams draining heterogeneous landscapes. (**a**) Climatic signals are filtered (e.g., scattered or attenuated) by the landscape and/or stream networks, resulting in reduced synchrony between stream pairs or the emergence of nonlinear synchrony responses across distance gradients. Red circles represent specific examples of streams exhibiting differences in pairwise characteristics: 1) geographical distance or linear proximity (i.e., from A-B to A-D), 2) land cover (LC) of the sub-catchment (e.g., A-C: LC1 vs. LC1; A-B: LC1 vs. LC2; A-D: LC1 vs. LC3), and 3) connectivity within the drainage network (e.g., A-B: streams not connected; A-C: streams connected longitudinally thought the main channel). (**b**) Synchrony can exhibit different manifestations across timescales due to mechanisms operating at specific temporal scales. Green and red solid lines represent simulated solute signal fluctuations for a specific parameter at two different stream

locations. In the first and third examples, the two streams exhibit synchrony for the specific parameter at the shorter period of the signal (Timescale 1). In contrast, in the second example, the two streams are synchronized at longer periods (Timescale 2) while showing asynchrony at the shorter timescale (Timescale 1). Figure 1(**b**) has been adapted from Defriez and Reuman (2017).

Methods

Study sites

We selected nine stream segments distributed across three catchments (Vallon de Nant, Valsorey and Val Ferret) in the Western region of the Swiss Alps (Figure S1). The selected streams and their corresponding catchments are located within a 40 km radius of each other (Figure S1a). While the proximity of these catchments leads to comparable meteorological patterns (e.g., temperature regimes and precipitation levels), they encompass a range of topo-climatic and environmental gradients characteristic of high-altitude systems (Figure S1b and Table S1). Among these streams, two (PEU and VEL) are not influenced by glaciers, while the remaining seven receive meltwaters from glaciers, which cover 3.4% to 33.5% of their catchments (Table S1). The drainage areas of these streams vary in size from 3.1 to 23.2 km^2. The catchment altitudes range from 1200 to 2161 m above sea level (a.s.l.) and stream channel slopes vary from 0.05 to 0.16 mm^{-1}. Six of the stream segments (VAU, VAD, VEL, FEU, FED and PEU) are situated above the tree line, draining steep slopes with sparsely vegetated rocky terrain with grassland and shrubs. In contrast, the remaining three (RIC, AND, ANU) drain partially forested catchments mainly composed of coniferous tree species. The total vegetation cover across the catchments ranges from 21.1% to 70.2% (Boix Canadell et al., 2019). The geological composition of the catchments exhibits certain variability. The Vallon de Nant catchment is dominated by limestones, calcareous shales, and flysch. In the Val Ferret catchment, the geology is primarily composed of limestones and sandstones with pronounced schistosity. In contrast, the Valsorey catchment stands out with its metamorphic lithology, including gneisses, crystalline shales, and blue-grey schists. These geological differences also contribute to the diverse characteristics and dynamics observed in the streams.

To assess the similarity between stream pairs, we calculated a similarity index based on geographical and landscape characteristics (Table S2). We considered six main characteristics: linear distance (or horizontal proximity), sub-catchment land cover, topographic attributes, and connectivity within the drainage network. The stream connectivity index was assigned a value of 2 when two streams were connected longitudinally through the main channel, 1 when one stream was a tributary of the main channel, and 0 when the stream segments were not connected or belonged to different catchments (Figure S1b). This analysis aimed to hypothesize which stream pairs would exhibit greater temporal coherence based on their geographic and landscape attributes.

Automated sensor measurements

At each stream segment, we deployed high-resolution sensors to measure parameters over a three-year period (from October 28, 2016, to October 20, 2019) as part of the ongoing METALP stream monitoring network (https://metalp.epfl.ch/). Sensors measured every ten minutes water depth (WT-HR 1000, TruTrack), chromophoric DOM (CDOM) sensor (Cyclops-7 CDOM/FDOM, PME Inc.), and turbidity (Cyclops-7 Turbidity, PME Inc.); all of them also measuring streamwater temperature. Before deployment, the optical sensors were calibrated in the laboratory according to the manufacturers' specifications. Turbidity sensors were calibrated using sensor-specific Turbidity NTU Calibration Standard-Formazin (Sigma-Aldrich®) up to 2000 NTU, and measurements were reported in nephelometric turbidity units (NTU). The CDOM sensor measured fluorescence and was calibrated in parts per billion (ppb) of quinine sulfate equivalents (fluorescence of 1 ppb quinine sulfate monohydrate (Sigma-Aldrich®) in 0.05 M H_2SO_4) using a two-point calibration curve (0 to 1,000 ppb quinine sulfate equivalents). Additionally, monthly spot measurements of the same parameters were conducted during site visits to validate the recorded data, assess data quality and eventually post-correct time series.

Discharge ($m^3\ s^{-1}$) was estimated using slug-injections of sodium chloride as a conservative tracer (Gordon et al. 2004). Rating curves relating streamwater depth to discharge were established for each site using a power-law model. The data was log-transformed, and a linear regression was performed to fit the rating curve equation. This approach allowed for the estimation of discharge based on water depth measurements obtained from the deployed sensors.

Relationships between streamwater FDOM and DOC concentrations

We compensated raw sensor FDOM data for streamwater temperature (FDOMtemp) and turbidity (FDOMcorr) as follows (Downing et al. 2012; Boix Canadell et al. 2019):

$$FDOM_{temp}=\frac{FDOM_{raw}}{1\text{-}0.016\ (Temp_m\text{-}Temp_{ref})} \qquad (1)$$

$$FDOM_{corr}=\frac{FDOM_{temp}}{0.95\ e^{(-0.002\ Turb_m)}+0.03} \qquad (2)$$

where $FDOM_{raw}$ refers to the uncorrected FDOM values, $Temp_m$ is the streamwater temperature, $Temp_{ref}$ is the reference temperature at 10 °C, and $Turb_m$ represents the streamwater turbidity (Watras et al. 2011; Lee et al. 2015). The coefficients were derived from laboratory experiments that assessed the sensor specific effect of temperature and turbidity on the FDOM signal. These coefficients were comparable to those reported in previously studies (Watras et al. 2011; Downing et al. 2012; Lee et al. 2015).

Additionally, we conducted regular site visits, with a minimum frequency of once a month for sensor maintenance, data downloading, and grab sampling for DOC analysis. Streamwater samples for DOC analysis were filtered using precombusted GF/F filters (Whatman) and collected in acid-washed, precombusted glass vials; DOC concentrations were analyzed using a Sievers M5310c TOC Analyzer (GE Analytical Instruments).

The time series of streamwater DOC concentrations were calculated through least-squares linear regressions between $FDOM_{corr}$ sensor data and DOC concentrations measured from grab samples (for more details on the methods, see Boix Canadell et al. 2019).

Wavelet coherence

We applied wavelet coherence (Torrence and Compo 1998; Grinsted et al. 2004; Schmidt et al. 2019) to identify synchronous fluctuations in Q and DOC concentration of stream pairs. To achieve this, we decomposed both time series using continuous wavelet transforms, which convert time series from the time domain to the time-frequency domain. The wavelet transform involves convolving a time series $x(t)$ with a wavelet $\psi(t)$, which is a basis function localized in both time and frequency. We selected the Morlet wavelet as the basis function, due to its balance between time and frequency resolution and its widespread usage (Torrence and Compo 1998; Cazelles et al. 2008; Cauvy-Fraunié et al. 2013; Schmidt et al. 2019; Kneib et al. 2020). The Morlet wavelet consists of a plane wave modulated by a Gaussian distribution and it defined as

$$\psi_0(\mathrm{t}) = \pi^{-\frac{1}{4}}\, \mathrm{e}^{-\mathrm{i}\omega_0 t}\mathrm{e}^{-\frac{t^2}{2}} \qquad (3)$$

where t represents time, and ω_0 is the central angular frequency. The continuous wavelet transform at scale f and time τ is given by:

$$|W(f, \tau)| = \frac{1}{\sqrt{f}}\int_{-\infty}^{+\infty} x(t)\psi^* \left(\frac{1-\tau}{f}\right) \mathrm{d}t = \int_{-\infty}^{+\infty} x(t)\psi_{f,\tau}^* \left(\frac{1-\tau}{f}\right) \mathrm{d}t \qquad (4)$$

where (*) denotes the complex conjugate form (Torrence and Compo 1998, Cazelles et al. 2008). In Layman's terms, the wavelet function can be considered a portion of a sine function, which is then compared to different segments of the time series of observables. In the next step, the frequency of the wavelet function is modified by compressing or extending it along the time axis. As a result, this wavelet provides specific information about frequency and time localization. Wavelet coherence is determined by squaring of the product of the wavelet transform of the first time series, $W_{f,\tau}^{X}$, with the complex conjugation of the second time series, $W_{f,\tau}^{X}$, and normalizing it by the individual power spectra of each time series (see Schmidt et al. 2019).

Wavelet coherence ranges between 0 and 1, and identifies phases of local cross-correlation between two time series as a function of frequency. High values of wavelet coherence indicate strong similarity between time series at a specific frequency and during a particular time window. All analyses were performed using R (R Core Team 2021). Wavelet coherence relationships were calculated using the R biwavelet package (Gouhier et al. 2018), which is based on MATLAB's WTC package (Grinsted et al. 2004). Starting from version 0.14, biwavelet also includes the plotting of bias-corrected wavelet and cross-wavelet power spectra, following the methods described by Liu et al. (2007) and Veleda et al. (2012). This correction is necessary because the traditional approach for computing the power spectrum (e.g., Torrence and Compo 1998) leads to an artificial and systematic reduction in power at lower periods. The significance of wavelet coherence was determined by comparing it to red noise, generated by 100 Monte Carlo randomizations of a first-order autoregressive process

(AR1) with the same autocorrelation coefficients as the respective input time series. Significance was tested at a significance level of 0.95.

We generated a total of thirty-six wavelet coherence and cross-wavelet power spectrums for both discharge and dissolved organic carbon using the methods described above. Due to the large number of graphs generated, we have included examples of the wavelet coherence spectrum for two stream pairs with contrasting synchrony patterns for discharge (Figure 2a and 2b) and for dissolved organic carbon concentrations (Figure 2c and 2d). The left panels of Figure 2 depict streams (VAU-VAD) with the highest pair similarity ranks for all geographic distance, sub-catchment land cover, and network connectivity (representing case A-C in Figure 1). The right panels of Figure 2 depict streams (VAU-FED) with relatively low pair similarity ranks for all geographic distance, sub-catchment land cover, and network connectivity (representing case A-D in Figure 1).

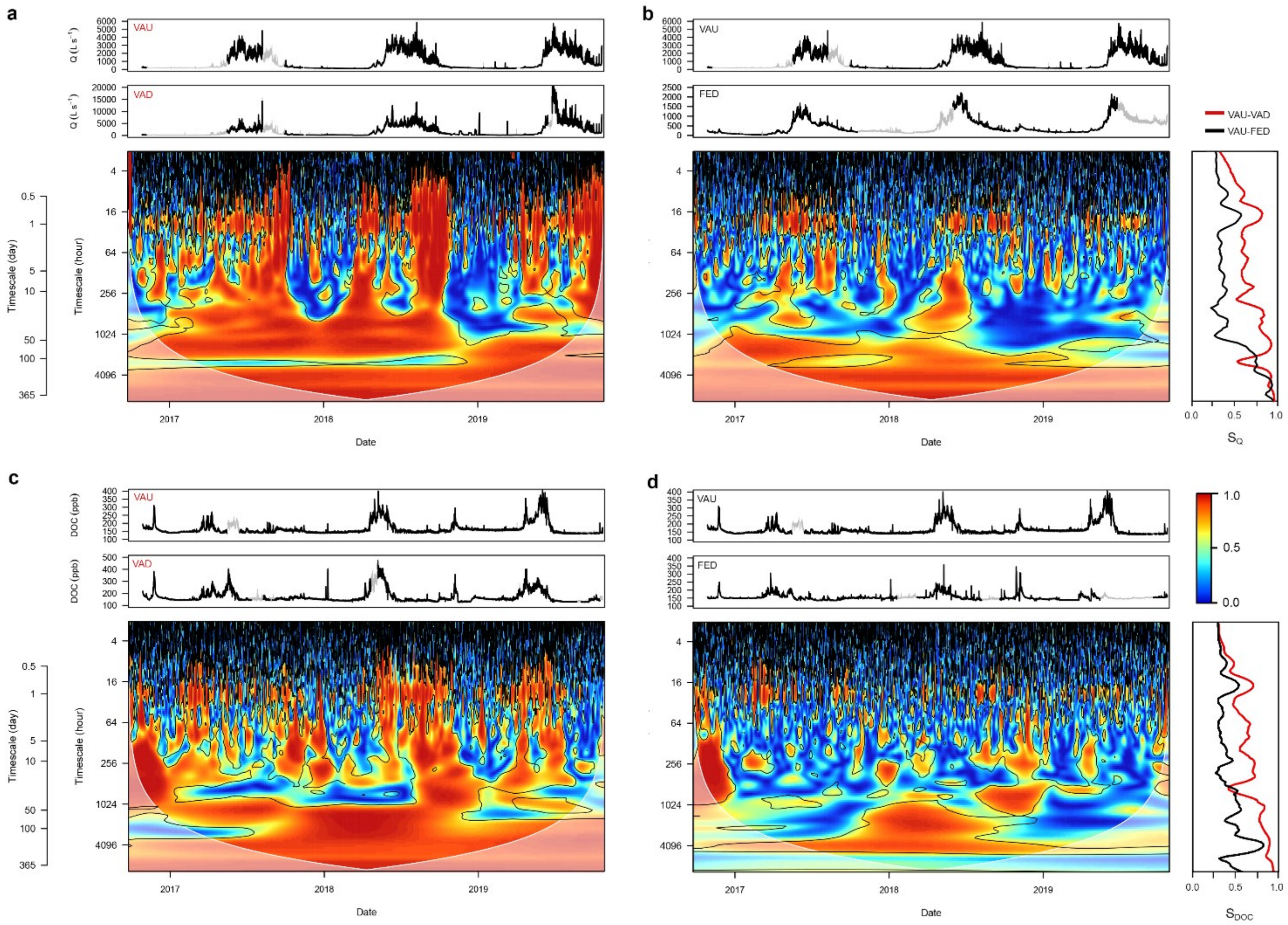

Figure 2. Time series and wavelet coherence spectrum of two contrasting stream pairs for discharge (**a, b**) and dissolved organic carbon concentration (**c, d**). The left panels compare streams VAU and VAD, which exhibit the highest pair similarity ranks across all geographic distances, sub-catchment land cover, and network connectivity (corresponding to case A-C in Figure 1). The right panels compare streams VAU and FED, which have relatively low pair similarity ranks for geographic distance, sub-catchment land cover, and network connectivity (corresponding to case A-D in Figure 1). In the time series plots, grey regions indicate data gaps that were imputed. The black contours represent regions of significant coherence against red noise, determined using Monte Carlo AR1 time series with a significance level of 0.95. The lighter shade denotes the cone of influence, where edge effects may distort coherence patterns. The y-axis on the coherence

spectrum indicates timescale length, expressed in both hours and days. The panels on the right margin display the global wavelet coherence or synchrony for discharge (S_Q, upper panel) and dissolved organic carbon (S_{DOC}, lower panel), calculated as the arithmetic mean over time.

Results and discussion

Timescale-aggregated synchrony

Timescale-aggregated synchrony, measured as the median synchrony across all timescales, ranged from 0.34 to 0.68 (median: 0.43, n=36) for discharge (S_Q) and from 0.25 to 0.62 (median: 0.36, n=36) for DOC (S_{DOC}) among stream pairs (Figure S2). Out of thirty-six stream pairs, thirty had higher aggregated S_Q than S_{DOC} (Figure S2). However, timescale aggregated S_Q than S_{DOC} was not significantly related ($r^2 = 0.10$; $p > 0.05$, n = 36; Figure S2). This low correlation is consistent with other studies showing that discharge fluctuations between streams are often more synchronous over spatial scales compared to soil-derived dissolved constituents (Basu et al. 2010; Thompson et al. 2011). Similar to water levels in lakes (Magnuson et al. 1990; Kratz et al. 1998), stream discharge dynamics are likely to be more directly influenced (i.e., less filtered) by climatic factors, whereas DOC concentrations are either indirectly influenced by climatic factors or interactively influenced (or filtered) by other localized factors such as soil production, atmospheric deposition, terrestrial-aquatic transfer, and internal processing.

Timescale-decomposed synchrony

Decomposition of timescale-aggregated synchrony revealed that both S_Q and S_{DOC} were strongly influenced by the timescale of fluctuations (Figure S3). As timescales increased from shorter to longer periods, both individual (Figure S3a and S3b) and averaged (Figure S3c) stream pair synchrony for Q and DOC showed a continuous increase (averaging from 0.24 to 0.94 for S_Q and from 0.27 to 0.82 for S_{DOC}; Figure S3c). The only exception to this pattern was a pronounced increase in both S_Q and S_{DOC} at the daily timescale, reflecting the synchronized response of these variables to daily climatic fluctuations (e.g., air temperature, solar radiation, soil evapotranspiration). At certain specific timescales, S_Q and S_{DOC} exhibited different responses (Figure 3a), with S_Q increasing more rapidly than S_{DOC} for timescales of approximately 50 days and beyond (Figure 3a). This difference becomes more pronounced when comparing short-term (0-50 days) and long-term (50-365 days) timescale bands, as S_Q increased from 0.32 to 0.68 while S_{DOC} remained relatively stable, at 0.31 to 0.33. This pattern suggests that regional landscape drivers have a relatively greater influence (or less filtration) on discharge fluctuations at longer timescales (e.g., beyond 50 days) compared to DOC fluctuations. In contrast, shorter-term fluctuations in both discharge and DOC (0-50 days) shared similar drivers.

In accordance with the previous pattern, the strength of the relationship between S_Q and S_{DOC} was also dependent on the timescale of fluctuations (Figure 3b). At shortest timescales (0-10 days), S_Q and S_{DOC} were significantly related ($r^2 = 0.58$; $p < 0.05$, n = 36;). However, this covariation between variables did not persist at timescales ranging from 10 to 50 days ($r^2 = 0.002$; $p > 0.05$, n = 36), 50 to 100 days ($r^2 = 0.001$; $p > 0.05$, n

= 36), or 100 to 365 days ($r^2 = 0.003$; $p > 0.05$, n = 36). Consistent with the aggregated data, the changing dynamics of S_Q and S_{DOC} from shorter to longer timescales suggest that mechanisms operating at shorter timescales (directly linked to climatic fluctuations) affect both variables similarly. However, the mismatch between S_Q and S_{DOC} observed at longer timescales suggests that DOC dynamics, which are likely more influenced by local catchment drivers, tend to be further removed from direct climate forcing or regional climatic divers. Although climate also influences the processes driving DOC patterns due to its intrinsic hydrological connection, many other local-scale processes, including soil DOC production, terrestrial-aquatic DOC transfer, and internal DOC processing, are likely filtering such signals (Li et al. 2018; Boix Canadell et al. 2019; Rosset et al. 2020).

The variability of S_Q and S_{DOC}, measured as the standard deviation (SD) of S_Q and S_{DOC} for the 36 stream pairs at each timescale, also increased significantly with the timescale of fluctuations. For S_Q, the SD ranged from 0.030 to 0.242, while for S_{DOC}, it ranged from 0.007 to 0.280. Notably, the threshold at which SD increased more markedly was approximately 10 days (Figure S3d). This consistent increase in dispersion suggests that controls on the variables are less constrained and more diversified (Abbott et al. 2018).

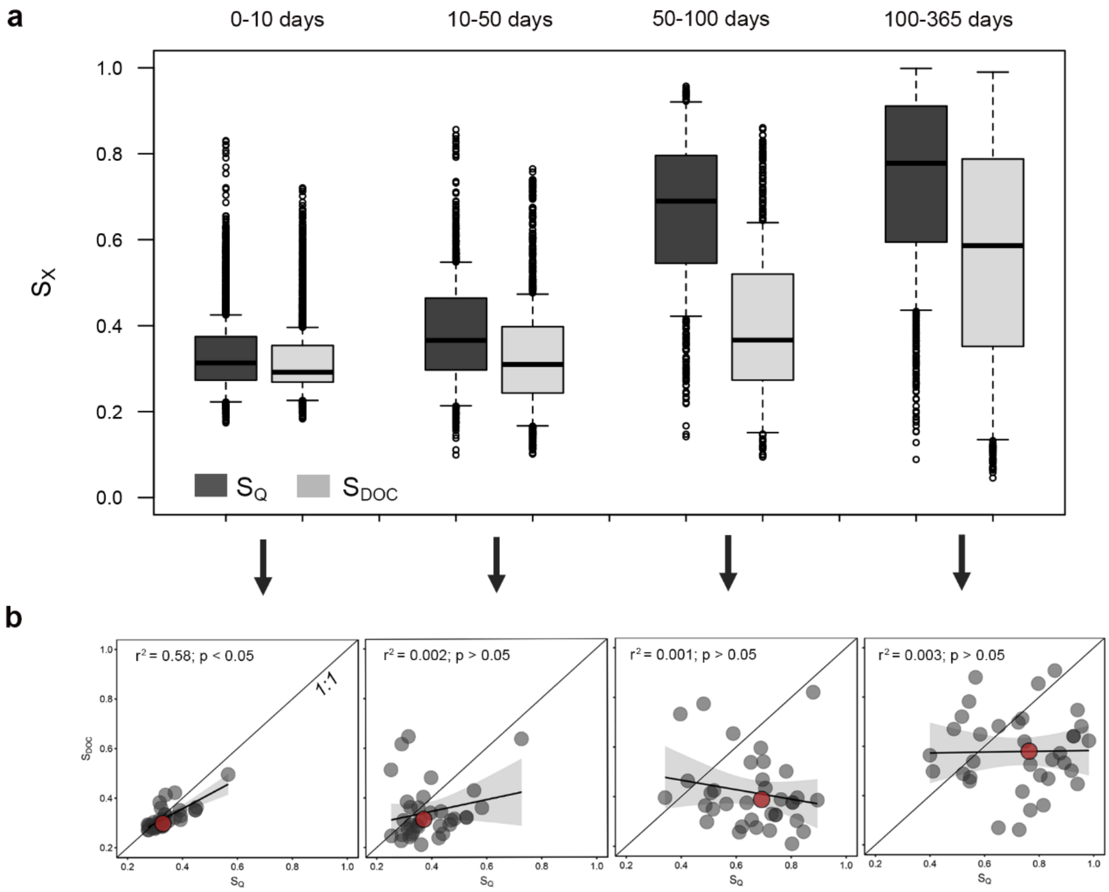

Figure 3. (a) Comparison and (**b**) relationships between aggregated S_Q and S_{DOC} at four specific timescale ranges (see headings). In panel **(a)** box plots display the 25th, 50th, and 75th percentiles; whiskers display 10th and 90th percentiles. In panel **(b)** red circles represent medians of the time-scale aggregated data, while lines represent least-squares linear

regression models between aggregated SQ and SDOC at four specific timescale ranges. The corresponding text provides statistical outputs (r^2 and p-values) for each regression model.

Spatial variability of synchrony

In our study region, streams that were closer to each other exhibited higher S_Q and S_{DOC} values compared to streams that are more spatially separated (Figure 4a and 4b). Therefore, consistent with Kling et al., 2000, timescale-aggregated S shows relatively low geographical persistence across the distance gradient (ranging from 0.1 to 40 km) for both Q and DOC (Figure 4a and 4b, respectively). As depicted in the conceptual model (Figure 1a, left panels), large-scale synchrony persistence can be attributed to the presence of strongly "regionalized" environmental variables, such as shared exposure to similar climatic shifts or homogeneous landscape properties. However, in our case, the observed trend of decreasing synchrony with spatial position suggests that localized controls are overriding or strongly influencing the effects of higher-scale drivers operating at the entire region and acting as synchrony stabilizers. These findings align with previous studies conducted in lake districts, where a negative correlation between lake pairs S and lake similarity in exposure to climatic factors (measured as pair distance and area/depth ratio) was moderate to high in most cases (Magnuson et al. 1990; Soranno 1999; Kling et al. 2000).

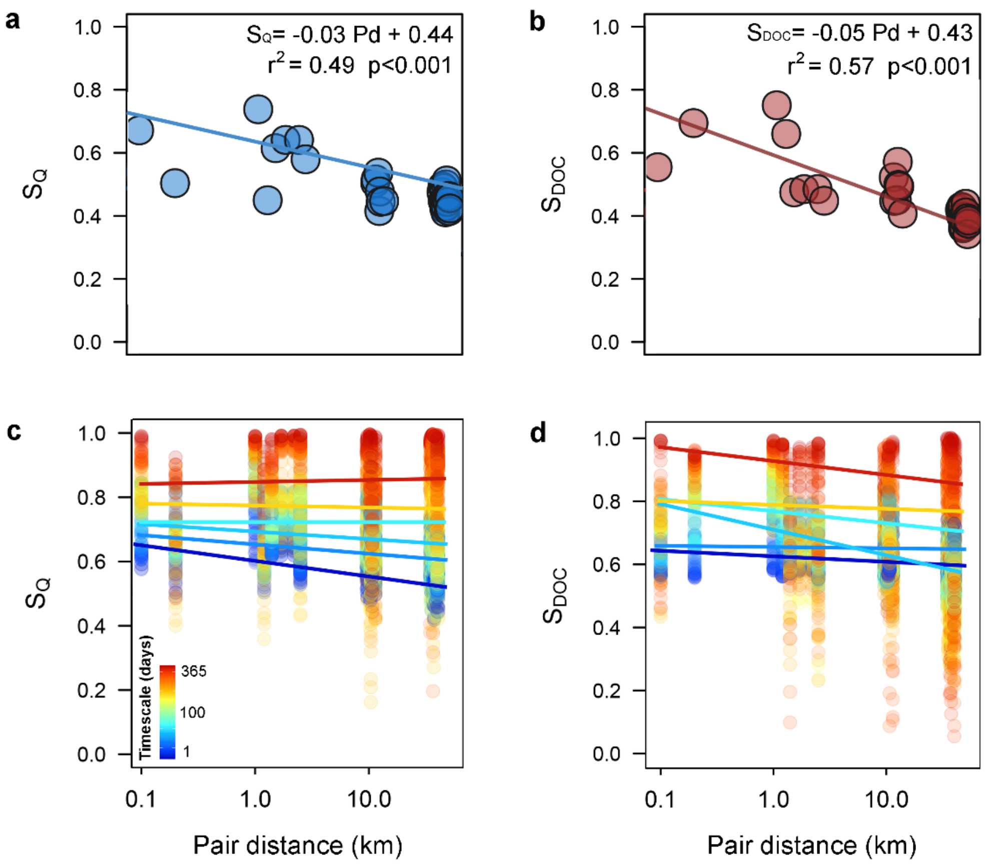

Figure 4. Relationships between timescale aggregated (**a**) S_Q and (**b**) S_{DOC} (measured as the median coherence between stream pairs for all timescales) and timescale segregated (**c**) S_Q and (**d**) S_{DOC} (measured as the median coherence of six specific timescale bands) and stream pair distance. Lines in panels **(a)**, **(b)**, **(c)** and **(d)** represent to least-squares linear

regression models. Refer to Table S4 for the statistical outputs of the least-squares linear regression models associated with panels (**c**) and (**d**).

In our study, the loss of synchrony with linear distance could be attributed to the local landscape heterogeneity characteristic of high-mountain regions. This heterogeneity includes differences in the size and arrangement of landscape patches that act as sources and sinks of water and solutes, such as DOC (e.g., soils, groundwater, snow, ground ice, and glaciers), which ultimately control the routing of water and the delivery of solutes to streams as water flows superficially and sub-superficially (Tank et al. 2018) through the landscape (Malard et al. 1999; Brown et al. 2003). Additionally, S_{DOC} may be uniquely influenced by the local effects of consistent processing, such as ecosystem respiration, as water flows within river ecosystems. If these interpretations are correct, we would expect the reduction of S with distance to be more pronounced or correlated for DOC. However, despite the slope of the relationship between timescale-aggregated S_{DOC} and pair distance being slightly higher than that for S_Q (Table S3), a regression analysis indicated that only S_{DOC} (not S_Q) was additionally influenced by local topographical and land cover properties, such as altitude and catchment vegetation coverage (Table S3).

In accordance with the timescale-aggregated data, negative correlations between S_{DOC} and stream pair distance persisted even after segregating the data by timescale (Figure 4c and 4d; Table S4). This pattern was more consistent at longer timescales of fluctuations and contrasted with the observations for S_Q, which exhibit higher spatial persistence at longer and intermediate timescales but showed higher correlation at shorter timescales (as described in the drivers below). Taken together, these results suggest that S_{DOC} dynamics are more sensitive to locally unique conditions compared to S_Q, and that these local conditions exert distinct effects on the variables across the range of explored timescales.

Timescale-dependent drivers of synchrony

Given that the magnitude and dynamics of S_Q and S_{DOC} depended on the timescale of observation, we hypothesized that the mechanisms driving synchrony would also vary across timescales. To investigate this, we conducted linear regression analysis to examine whether potential drivers of S_Q and S_{DOC} (Figure 1a and Table S1) operated differently at each specific timescale considered (n=148, ranging from 1 hour to 365 days). The statistical outputs from these models provided evidence that the mechanisms driving S_Q and S_{DOC} dynamics indeed differed across timescales (Figure 5). Considered drivers were stream pair distance, network connectivity, and altitude, glacier extent and vegetation cover (hereafter catchment properties). At short timescales (ranging from 0 to 10 days), S_Q and S_{DOC} were strongly correlated with stream pair distance (median r^2_Q=0.40, r^2_{DOC}=0.41) and network connectivity (median r^2_Q=0.30, r^2_{DOC}=0.21), while weaker relationships were observed with catchment-related properties within the same timescale range (median r^2_Q=0.08, r^2_{DOC}=0.10). Similarly, at timescales ranging from 10 to 50 days, stream pair distance (median r^2_Q=0.11, r^2_{DOC}=0.37) and network connectivity (median r^2_Q=0.20, r^2_{DOC}=0.14) remained the most important factors driving S_Q and S_{DOC} (Figure 5). These results indicate that linear proximity and connectivity between stream pairs, either through the landscape or the stream network, controlled short-term S dynamics regardless the differences in local landscape characteristics observed between the catchments they drain (Table S1 and S2).

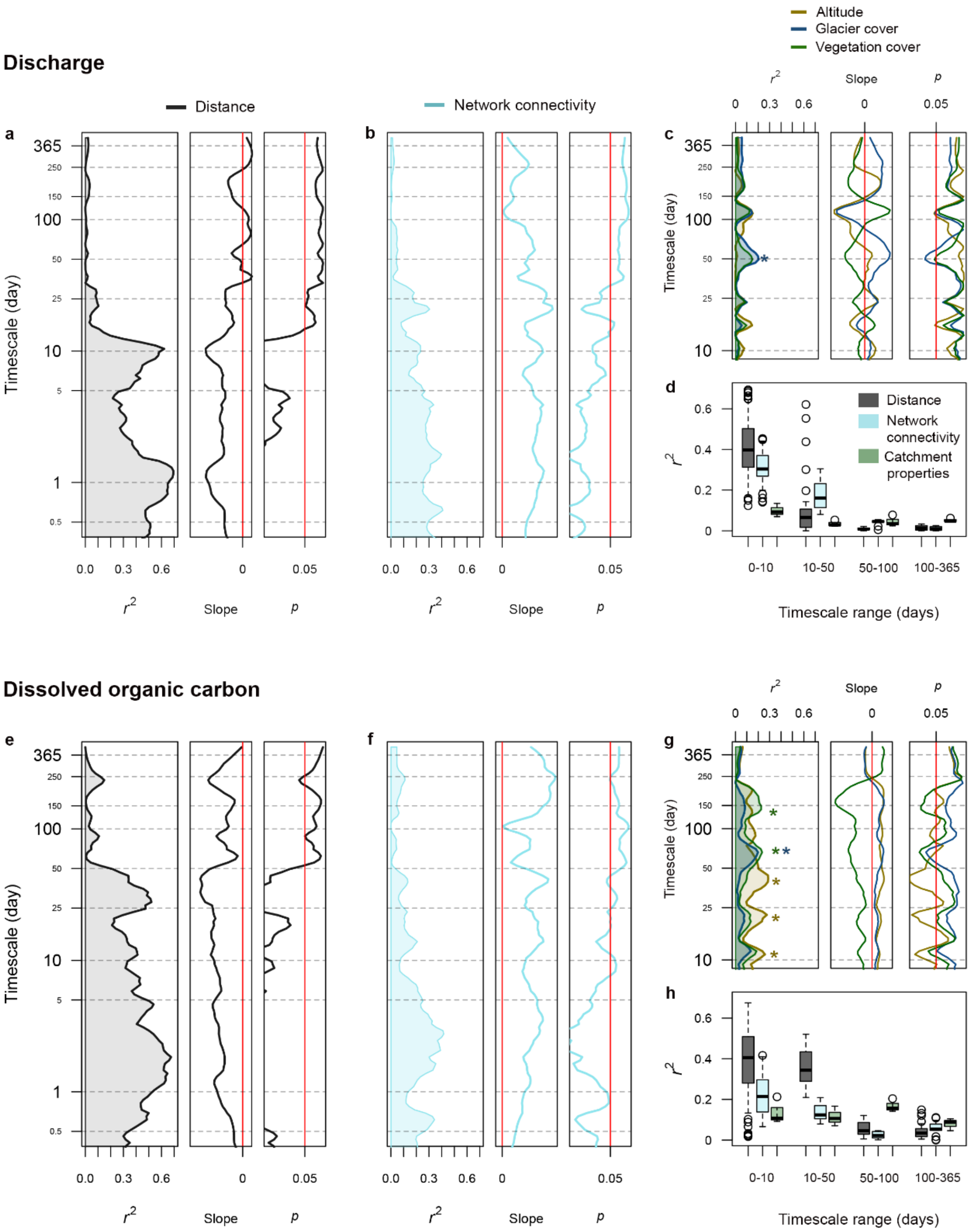

Figure 5. Temporal (or timescale) structure of the spatial drivers of (a) discharge synchrony (SQ) and (b) dissolved organic carbon synchrony (SDOC). Linear regression models were used to assess relationship between SQ and SDOC and each explanatory variable (distance, network connectivity, catchment altitude, catchment glacier extent and catchment vegetation cover) for each timescale or period evaluated. A total of 148 models were analyzed, corresponding to 148 periods ranging from 0.5 to 365 days. Statistical parameters including r^2, slope and p-values are provided for each model. The horizontal dashed lines represent reference timescales, while vertical red lines indicate the reference slope (at slopes of 0) and significance level (p-value < 0.05). Asterisks in the top right panels indicate statistically significant variables

for specific time periods. Boxplots summarize the proportion of variance (r^2) on the dependent variable (SQ and SDOC) explained by each group of independent variables. The averages are presented for specific categories described in Figure 1a, namely distance, network connectivity, and catchment properties, within four specific timescale windows (i.e., 1-10, 10-50, 50-100, and 100-365 days).

This shared control of S_Q and S_{DOC} suggests a coupled responsiveness of Q and DOC dynamics to different processes associated with regional physical weather dynamics, including short-term fluctuations in air temperature, solar radiation, rain events, as well as intermediate-term fluctuations associated with cold fronts, ice or snow melting episodes. Interestingly, the influence of pair distance on S dynamics extended up to timescales of approximately 50 days for DOC, while it appeared to diminish after around 10 days for Q. In most of the studied headwaters, DOC export is primarily limited by hydrological transport during mobilization events meaning that additional sources of DOC are mobilized as discharge increases (Zarnetske et al. 2018; Boix Canadell et al. 2019). This finding supports the observed decoupling between S_Q and S_{DOC} synchrony dynamics within considered timescales.

For timescales longer than 50 days, the coefficient of determination (r^2) derived from the regression models including local catchment properties as explanatory variables, was higher than those with stream pair distance and network connectivity (Figures 5d and 5h). The extent to which local catchment properties controlled synchrony patterns at the longest timescales depended on both the type of response variable (S_Q versus S_{DOC}) and the specific nature of the catchment property (altitude versus vegetation cover versus glacier extent). Specifically, the effect of catchment properties on driving the S patterns at the longest timescales was significantly stronger for S_{DOC} (median r^2_{DOC}=0.17) than for S_Q (median r^2_Q=0.04). In terms of intra-catchment variations, relative glacier extent emerged as the most important variable driving higher S_Q at the longest timescales (Figure S4c and S4d), while vegetation cover, together with altitude, explained most of the variation in S_{DOC} for the same timescale bands (Figure S4g and S4h). Fluctuations at timescales longer than 50 days can be attributed to two major regional signals. First, spring snowmelt drives high spring discharge and associated DOC transport. Snowmelt is recognized as one of the major drivers determining inter-annual and seasonal dynamics in lake districts (e.g., Soranno 1999; Baines et al. 2000). Second, glacier ablation results in elevated glacier runoff and likely increases in DOC yield (Milner et al. 2017). In fact, upon melting, ice locked DOC can contribute to the downstream DOC pool (Singer et al. 2012; Hood et al. 2015; Li et al. 2018). Additionally, temperature seasonality across the studied region can lead to large seasonal variations in evapotranspiration, which in turn influences observed S patterns in Q and DOC by regulating the composition and fluxes of DOC. Finally, other landscape-dependent regional drivers of S have been identified in other studies, such as droughts, El Nino events, atmospheric deposition of DOC, although their role in determining synchrony is still being explored (Dillon and Molot 1997; Futter et al. 2007).

Our findings demonstrated that the difference in vegetation cover between stream pairs, but not the glacier extent, was negatively correlated with S_{DOC} at the longest timescales (Figure S4g, S4h). This pattern is consistent with a diversification of vegetation cover classes in the lower altitude catchments below the tree line. On the other hand, headwater catchments covered with similar vegetation classes in the highest parts of the studied area (i.e., more homogeneous areas covered by moors and mineral surfaces) exhibited more synchronized inter-annual DOC fluctuations. Unexpectedly, the seasonal fluctuations associated with glacier ablation drove S_Q patterns but not S_{DOC}. This result suggests that S_Q dynamics are retained regardless the variability in glacier extent, whether the streams are subject to more less or non-glacier ablation activity. However, this does not hold true for DOC. One possible explanation is that the amount of DOC transported by glacier-fed streams is not sufficient or has a source limitation, leading to a lack of homogenization in the S_{DOC} responses. In other words, the temporal pattern of DOC transported by non-glacier-fed streams, which drain forested catchments with more groundwater and rain contribution during periods of maximum glacier ablation (Malard et al., 1999; Tockner et al., 2002), is markedly different and does not overlap seasonally with that from glacier-fed streams. Ultimately, using a simple space-for-time substitution approach, we predict that at seasonal and inter-annual scales, S might decrease for Q but increase for DOC as glaciers shrink and high-mountain trees migrate to higher altitudes.

Time-series of synchrony from two neighboring streams

To exemplify how processes operating at multiple spatial scales drive the temporal structure (or timescale structure) of stream S_Q and S_{DOC} patterns in high mountains (as discussed in previous section), we analyzed the time series of synchrony for two of our streams (VAU and VEL, Figure S1) across five specific timescale ranges (1, 1-10, 10-50, 50-100, and 100-365 days; Figures 6 and S5S_{DOC} and S_Q, respectively). These two streams represent an extreme case of similarity in their exposure to climatic factors (measured as horizontal proximity; Table S1 and S2), but they differ significantly in their sub-catchment land cover and hydro-geomorphological attributes (e.g., the relative influence of glacier to vegetated drainage area in the catchment; Table S1 and S2). As a reference for the maximum expected pair synchrony, we also conducted the same analysis for two streams (VAU and VAD; Figure S1, Table S1 and S2) that showed the highest similarity indices for both exposure to climatic factors and sub-catchment attributes. This comparison aims to address how S_{DOC} and S_Q change in high-mountain streams throughout a typical hydrological cycle (including snowmelt, glacier ablation, and base flow dynamics), but varies across the five specific timescale ranges.

At the 1-day and 1- to 10-day timescale bands, the median S_{DOC} between VAU (glacier-fed stream; *G*) and VEL (non-glacier-fed stream; *NG*) was 0.63 and 0.49 respectively. These values were comparable to the S_{DOC} between VAU (*G*) and VAD (*G*) (0.68 and 0.64, respectively; Figure 6). This relatively high agreement between stream pairs subjected to different glacier influences (*G-G* vs. *G-NG*) confirms the role of landscape position (or proximity) in determining short-term S_{DOC} dynamics. However, each of the two stream pairs exhibited a unique seasonal pattern in S_{DOC}. While both stream pairs showed the highest S_{DOC} during the initial part of the snowmelt period (as shown in the left inset), differences in S_{DOC} were observed between the two pairs for the rest of the studied periods. For example, the largest differences in S_{DOC} between the two pairs (*G-G* vs. *G-NG*) were observed during the glacial ablation period when the S_{DOC} for the *G-NG* pair was the lowest, while for the *G-G* pair, it peaked most of the time (as shown in the right inset).

Consistent with our previous results, the difference in S_{DOC} between the two stream pairs (*G-G* vs. *G-NG*) increased significantly at timescales longer than 10 days. Specifically, the median S_{DOC} between VAU (*G*) and VEL (*NG*) was 0.47, 0.2, and 0.14, while between VAU (*G*) and VAD (*G*) it was 0.6, 0.85, and 0.95 for the timescale ranges of 10-50, 50-100, and 100-365 days, respectively. This more detailed exploration confirms that larger differences in local landscape attributes reduce S_{DOC} at the longest timescales. Importantly, the low synchrony between G-NG at the timescale associated with glacial ablation activity (while high S for the *G-G* pair) further indicates that glaciers play a significant role in desynchronizing DOC dynamics in high-mountain regions. Our findings show that glaciers impose a unique seasonal regime on DOC, which likely overrides the effects of other local hydrological or biogeochemical processes occurring during downstream transport within the main channel or between the main channel and the floodplain (Singer et al. 2012; Hood et al. 2015; Li et al. 2018; Boix Canadell et al. 2019). In contrast, groundwater-fed streams in high-mountain landscapes (such as VEL, used for comparison), are typically characterized by a relatively constant DOC concentration regime (Malard et al. 1999; Tockner et al. 2002), particularly during the glacial ablation period when they show little seasonal fluctuation compared to glacier-fed streams. Instead, they are mainly driven by short-scale fluctuations coinciding with rain events (Figure 6). Unlike the pattern of decreasing median S_{DOC} with timescale observed between VAU and VEL, the median S_Q remained relatively high across all the explored temporal ranges, resulting in a reduced difference with the reference pair (Figure S5). This observation, using two contrasting neighboring streams, is consistent with the previous results obtained from all the stream pairs. Additionally, the S_Q time series for the two studied stream pairs differed from that of S_{DOC}, especially at the shorter timescales (1 and 1-10 timescale ranges). In this case, apart from some specific events (as shown in the right inset), the overall coherence between the contrasting and reference stream pairs remained high and relatively consistent throughout most of the year.

Conclusions

Our study provides valuable insights into the temporal dynamics and synchrony patterns of discharge (S_Q) and dissolved organic carbon (S_{DOC}) in high-mountain streams. Through a comprehensive analysis of multiple timescales, a deeper understanding of the underlying processes driving the dynamics of S_Q and S_{DOC} has been achieved. We identified distinct mechanisms driving S_Q and S_{DOC} dynamics at different timescales. At shorter timescales, stream pair distance and network connectivity have emerged as important factors influencing S_Q and S_{DOC}, highlighting the role of linear proximity and connectivity. At longer timescales, local catchment properties (e.g., altitude, vegetation cover, and glacier extent) exert stronger control on synchrony patterns. The differential responses of S_Q and S_{DOC} to these catchment properties underscore the unique dynamics of these variables and their sensitivity to local conditions.

The study also contributes to our understanding of the interplay between glaciers and stream dynamics. Glacier extent induces a significant desynchronizing effect on S_{DOC} dynamics, resulting in reduced synchrony between glacier-fed and non-glacier-fed streams at longer timescales. This highlights the dominant influence of glaciers on the seasonal regime and variability of stream DOC concentration. Moreover, our study reveals the limitations of the spatial scalability of S_{DOC} synchrony, suggesting that the concept of sentinel ecosystems cannot be directly applied to headwater streams in high-mountain regions due to the low spatial persistence of S_{DOC} patterns. It is important to note that our study focuses on a portion of the Swiss Alps, and the extent and arrangement of landscape features, such as glacierized and post-glacierized areas, may vary in other high-mountain regions. This suggests that landscape synchrony dynamics within and beyond the study area may exhibit even greater heterogeneity. Nevertheless, the findings contribute to the fundamental understanding of the processes shaping high-mountain stream dynamics, providing insights into the intricate interplay between climate, hydrology, and landscape characteristics.

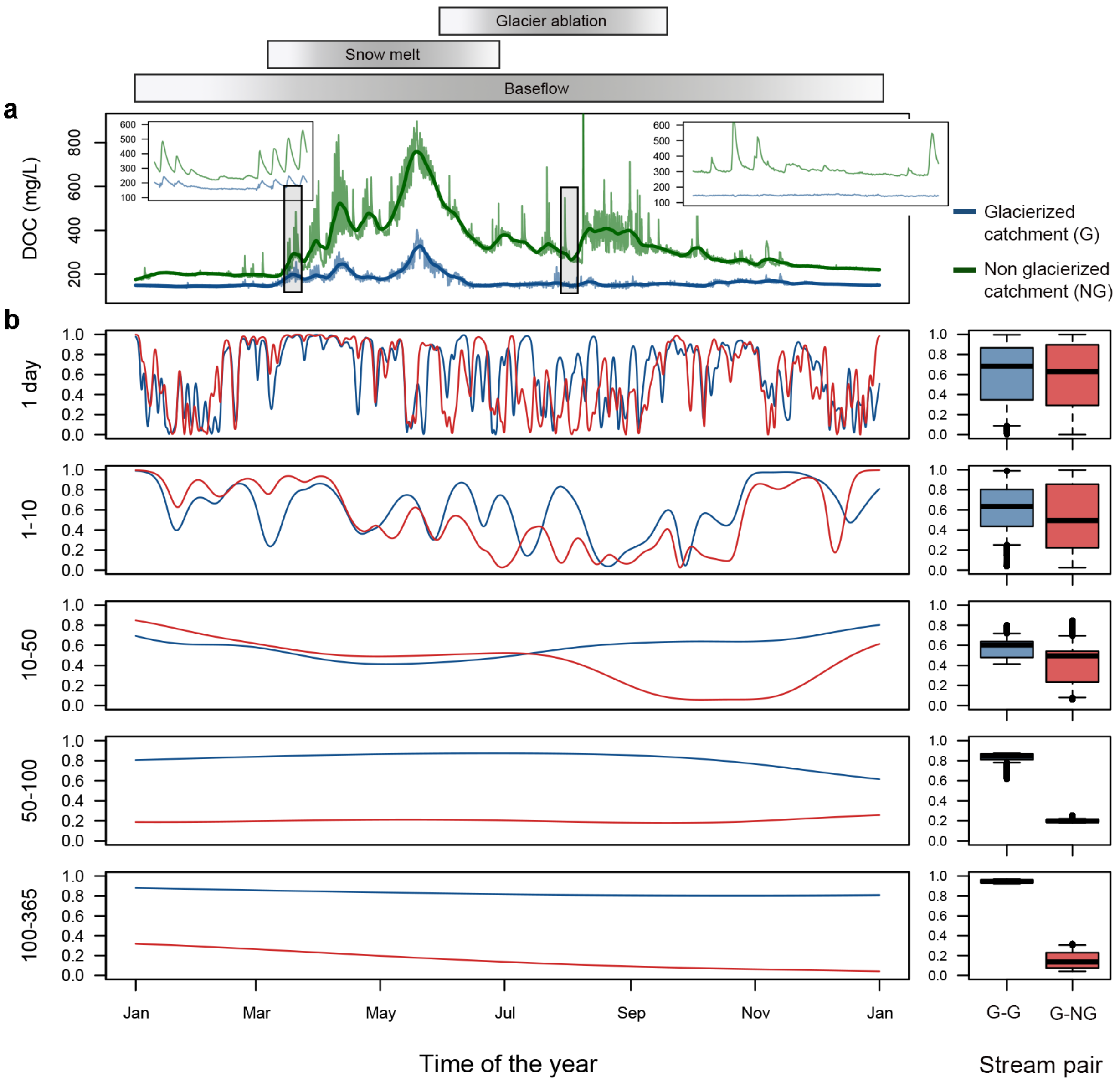

Figure 6. High-frequency time series of DOC (**a**) concentrations and (**b**) synchrony (S_{DOC}) between two selected stream pairs across five specific timescale ranges (1, 1-10, 10-50, 50-100 and 100-365 days). The first pair (VAU and VEL) consists of two neighboring streams (Figure S1) with contrasting sub-catchment land cover and hydro-geomorphological attributes (Table S1 and S2). VAU is influenced by glacier ice melt dynamics (G), while VEL is a groundwater-fed stream

draining a non-glacierized catchment (NG). In contrast, the two streams of the second pair (VAU and VAD), both influenced by glacier dynamics (G), exhibit the highest similarity indices for exposure to climatic factors and sub-catchment attributes (Table S1 and S2) and are used as a reference for maximum expected pair S. The right panels feature boxplots comparing differences in S between stream pairs (G-G vs. G-NG) at the five specific timescale ranges. The boxplots display the 25th, 50th, and 75th percentiles; whiskers represent the 10th and 90th percentiles.

Acknowledgments

This study was supported by funding (163015) from the Swiss Science Foundations to T.B. L.G. was further supported by a fellowship from ”la Caixa” Foundation (ID 100010434) and from the European Union's Horizon 2020 research and innovation programme under the Marie Skłodowska Curie grant agreement No 847648 (fellowship: LCF/BQ/PI21/11830034). We acknowledge all RIVER present and former collaborators for their precious help in both field and lab.

Author Contribution Statement

L.G.-G. and T.B. conceived the study and wrote the paper with input from N.D. L.G.-G. and N.D. compiled, processed and analyzed the data. All authors contributed with data and commented on the earlier versions of this manuscript.

Data Availability Statement

The data that support the findings of this study are available through the METALP data (https://metalp.epfl.ch/; https://doi.org/10.6084/m9.figshare.23522856.v3).

References

Abbott, B. W., G. Gruau, J. P. Zarnetske, and others. 2018. Unexpected spatial stability of water chemistry in headwater stream networks J. Grover [ed.]. Ecol Lett **21**: 296–308. doi:10.1111/ele.12897

Anderson, T. L., L. W. Sheppard, J. A. Walter, S. P. Hendricks, T. D. Levine, D. S. White, and D. C. Reuman. 2019. The dependence of synchrony on timescale and geography in freshwater plankton. Limnol Oceanogr **64**: 483–502. doi:10.1002/lno.11054

Baines, S. B., K. E. Webster, T. K. Kratz, S. R. Carpenter, and J. J. Magnuson. 2000. SYNCHRONOUS BEHAVIOR OF TEMPERATURE, CALCIUM, AND CHLOROPHYLL IN LAKES OF NORTHERN WISCONSIN. Ecology **81**: 815–825. doi:10.1890/0012-9658(2000)081[0815:SBOTCA]2.0.CO;2

Basu, N. B., G. Destouni, J. W. Jawitz, and others. 2010. Nutrient loads exported from managed catchments reveal emergent biogeochemical stationarity: BIOGEOCHEMICAL STATIONARITY. Geophys. Res. Lett. **37**: n/a-n/a. doi:10.1029/2010GL045168

Boix Canadell, M., N. Escoffier, A. J. Ulseth, S. N. Lane, and T. J. Battin. 2019. Alpine Glacier Shrinkage Drives Shift in Dissolved Organic Carbon Export From Quasi-Chemostasis to Transport Limitation. Geophys. Res. Lett. **46**: 8872–8881. doi:10.1029/2019GL083424

Brown, L. E., D. M. Hannah, and A. M. Milner. 2003. Alpine Stream Habitat Classification: An Alternative Approach Incorporating the Role of Dynamic Water Source Contributions. Arctic, Antarctic, and Alpine Research **35**: 313–322. doi:10.1657/1523-0430(2003)035[0313:ASHCAA]2.0.CO;2

Cauvy-Fraunié, S., T. Condom, A. Rabatel, M. Villacis, D. Jacobsen, and O. Dangles. 2013. Technical Note: Glacial influence in tropical mountain hydrosystems evidenced by the diurnal cycle in water levels. Hydrol. Earth Syst. Sci. **17**: 4803–4816. doi:10.5194/hess-17-4803-2013

Cazelles, B., M. Chavez, D. Berteaux, F. Ménard, J. O. Vik, S. Jenouvrier, and N. C. Stenseth. 2008. Wavelet analysis of ecological time series. Oecologia **156**: 287–304. doi:10.1007/s00442-008-0993-2

Defriez, E. J., D. C. Reuman, and D. Tittensor. 2017. A global geography of synchrony for marine phytoplankton. Global Ecol Biogeogr **26**: 867–877. doi:10.1111/geb.12594

Defriez, E. J., L. W. Sheppard, P. C. Reid, and D. C. Reuman. 2016. Climate change-related regime shifts have altered spatial synchrony of plankton dynamics in the North Sea. Glob Change Biol **22**: 2069–2080. doi:10.1111/gcb.13229

Dillon, P. J., and L. A. Molot. 1997. Dissolved Organic and Inorganic Carbon Mass Balances in Central Ontario Lakes. Biogeochemistry **36**: 29–42.

Downing, B. D., B. A. Pellerin, B. A. Bergamaschi, J. F. Saraceno, and T. E. C. Kraus. 2012. Seeing the light: The effects of particles, dissolved materials, and temperature on in situ measurements of DOM fluorescence in rivers and streams: Effects and compensation for in situ DOM fluorescence. Limnol. Oceanogr. Methods **10**: 767–775. doi:10.4319/lom.2012.10.767

Fisher, S. G., N. B. Grimm, E. Martí, R. M. Holmes, and J. B. J. Jr. 1998. Material Spiraling in Stream Corridors: A Telescoping Ecosystem Model. Ecosystems **1**: 19–34. doi:10.1007/s100219900003

Frissell, C. A., W. J. Liss, C. E. Warren, and M. D. Hurley. 1986. A hierarchical framework for stream habitat classification: Viewing streams in a watershed context. Environmental Management **10**: 199–214. doi:10.1007/BF01867358

Futter, M. N., D. Butterfield, B. J. Cosby, P. J. Dillon, A. J. Wade, and P. G. Whitehead. 2007. Modeling the mechanisms that control in-stream dissolved organic carbon dynamics in upland and forested catchments: MODELING SURFACE WATER DOC. Water Resour. Res. **43**. doi:10.1029/2006WR004960

Gene E. Likens. 1989. Long-Term Studies in Ecology, Springer New York.

Gómez-Gener, L., E. R. Hotchkiss, H. Laudon, and R. A. Sponseller. 2021. Integrating Discharge-Concentration Dynamics Across Carbon Forms in a Boreal Landscape. Water Res **57**. doi:10.1029/2020WR028806

Gordon, N. D., T. F. Allnutt, B. L. Finlayson, C. J. Gippel, and R. J. Nathan. 2004. Stream hydrology: An introduction for ecologists, John Wiley & Sons Inc.

Gouhier, T. C., A. Grinsted, and V. Simko. 2018. R package biwavelet: Conduct univariate and bivariate wavelet analyses (Version 0.20.17). Available from https://github.com/tgouhier/biwavelet.

Grinsted, A., J. C. Moore, and S. Jevrejeva. 2004. Application of the cross wavelet transform and wavelet coherence to geophysical time series. Nonlin. Processes Geophys. **11**: 561–566. doi:10.5194/npg-11-561-2004

Hampton, S. E., M. D. Scheuerell, M. J. Church, and J. M. Melack. 2019. Long-term perspectives in aquatic research. Limnol Oceanogr **64**. doi:10.1002/lno.11092

Hood, E., T. J. Battin, J. Fellman, S. O'Neel, and R. G. M. Spencer. 2015. Storage and release of organic carbon from glaciers and ice sheets. Nature Geosci **8**: 91–96. doi:10.1038/ngeo2331

Hynes, H. B. N. 1975. The stream and its valley., Verhandlungen der Internationalen Vereinigung fu¨r theoretische und angewandte Limnologie.

Kirchner, J. W., X. Feng, C. Neal, and A. J. Robson. 2004. The fine structure of water-quality dynamics: the(high-frequency) wave of the future. Hydrol. Process. **18**: 1353–1359. doi:10.1002/hyp.5537

Kling, G. W., G. W. Kipphut, M. M. Miller, and W. JohN. O'Brien. 2000. Integration of lakes and streams in a landscape perspective: the importance of material processing on spatial patterns and temporal coherence. Freshwater Biol **43**: 477–497. doi:10.1046/j.1365-2427.2000.00515.x

Kneib, M., S. Cauvy-Fraunié, N. Escoffier, M. Boix Canadell, Å. Horgby, and T. J. Battin. 2020. Glacier retreat changes diurnal variation intensity and frequency of hydrologic variables in Alpine and Andean streams. Journal of Hydrology **583**: 124578. doi:10.1016/j.jhydrol.2020.124578

Kratz, T. K., P. A. Soranno, B. J. Benson, and R. C. Lathrop. 1998. Interanual synchronous dynamics in north temperate lakes in Wisconsin, USA. Management of lakes and reservoirs during global climate change **42**: 273–287.

Lee, E.-J., G.-Y. Yoo, Y. Jeong, K.-U. Kim, J.-H. Park, and N.-H. Oh. 2015. Comparison of UV–VIS and FDOM sensors for in situ monitoring of stream DOC concentrations. Biogeosciences **12**: 3109–3118. doi:10.5194/bg-12-3109-2015

Levin, S. A. 1992. The Problem of Pattern and Scale in Ecology: The Robert H. MacArthur Award Lecture. Ecology **73**: 1943–1967. doi:10.2307/1941447

Li, X., Y. Ding, J. Xu, and others. 2018. Importance of Mountain Glaciers as a Source of Dissolved Organic Carbon. J. Geophys. Res. Earth Surf. **123**: 2123–2134. doi:10.1029/2017JF004333

Magnuson, J. J., B. J. Benson, and T. K. Kratz. 1990. Temporal coherence in the limnology of a suite of lakes in Wisconsin, U.S.A. Freshwater Biol **23**: 145–159. doi:10.1111/j.1365-2427.1990.tb00259.x

Malard, F., K. Tockner, and J. V. Ward. 1999. Shifting Dominance of Subcatchment Water Sources and Flow Paths in a Glacial Floodplain, Val Roseg, Switzerland. Arctic, Antarctic, and Alpine Research **31**: 135–150. doi:10.1080/15230430.1999.12003291

Marcé, R., G. George, P. Buscarinu, and others. 2016. Automatic High Frequency Monitoring for Improved Lake and Reservoir Management. Environ. Sci. Technol. **50**: 10780–10794. doi:10.1021/acs.est.6b01604

McGuire, K. J., C. E. Torgersen, G. E. Likens, D. C. Buso, W. H. Lowe, and S. W. Bailey. 2014. Network analysis reveals multiscale controls on streamwater chemistry. Proc. Natl. Acad. Sci. U.S.A. **111**: 7030–7035. doi:10.1073/pnas.1404820111

Milner, A. M., K. Khamis, T. J. Battin, and others. 2017. Glacier shrinkage driving global changes in downstream systems. Proc. Natl. Acad. Sci. U.S.A. **114**: 9770–9778. doi:10.1073/pnas.1619807114

Rode, M., A. J. Wade, M. J. Cohen, and others. 2016. Sensors in the Stream: The High-Frequency Wave of the Present. Environ. Sci. Technol. **50**: 10297–10307. doi:10.1021/acs.est.6b02155

Rosset, T., S. Binet, J.-M. Antoine, E. Lerigoleur, F. Rigal, and L. Gandois. 2020. Drivers of seasonal- and event-scale DOC dynamics at the outlet of mountainous peatlands revealed by high-frequency monitoring. Biogeosciences **17**: 3705–3722. doi:10.5194/bg-17-3705-2020

Schmidt, S. R., G. Lischeid, T. Hintze, and R. Adrian. 2019. Disentangling limnological processes in the time-frequency domain. Limnol. Oceanogr. **64**: 423–440. doi:10.1002/lno.11049

Sheppard, L. W., J. R. Bell, R. Harrington, and D. C. Reuman. 2016. Changes in large-scale climate alter spatial synchrony of aphid pests. Nature Clim Change **6**: 610–613. doi:10.1038/nclimate2881

Singer, G. A., C. Fasching, L. Wilhelm, J. Niggemann, P. Steier, T. Dittmar, and T. J. Battin. 2012. Biogeochemically diverse organic matter in Alpine glaciers and its downstream fate. Nature Geosci **5**: 710–714. doi:10.1038/ngeo1581

Soranno, P. A. 1999. Spatial Variation among Lakes within Landscapes: Ecological Organization along Lake Chains. Ecosystems **2**: 395–410. doi:10.1007/s100219900089

Tank, S. E., J. B. Fellman, E. Hood, and E. S. Kritzberg. 2018. Beyond respiration: Controls on lateral carbon fluxes across the terrestrial-aquatic interface: Controls on lateral carbon fluxes. Limnol. Oceanogr. **3**: 76–88. doi:10.1002/lol2.10065

Thompson, S. E., N. B. Basu, J. Lascurain, A. Aubeneau, and P. S. C. Rao. 2011. Relative dominance of hydrologic versus biogeochemical factors on solute export across impact gradients: HYDROLOGY CONTROLS SOLUTE EXPORT. Water Resour. Res. **47**. doi:10.1029/2010WR009605

Tockner, K., F. Malard, U. Uehlinger, and J. V. Ward. 2002. Nutrients and organic matter in a glacial river-floodplain system (Val Roseg, Switzerland). Limnol. Oceanogr. **47**: 266–277. doi:10.4319/lo.2002.47.1.0266

Torrence, C., and G. P. Compo. 1998. A Practical Guide to Wavelet Analysis. Bulletin of the American Meteorological Society **79**: 18.

Turner, M. G., V. H. Dale, and R. H. Gardner. 1989. Predicting across scales: Theory development and testing. Landscape Ecol **3**: 245–252. doi:10.1007/BF00131542

Vannote, R. L., G. W. Minshall, K. W. Cummins, J. R. Sedell, and C. E. Cushing. 1980. The River Continuum Concept. Can. J. Fish. Aquat. Sci. **37**: 130–137. doi:10.1139/f80-017

Walter, J. A., L. W. Sheppard, T. L. Anderson, J. H. Kastens, O. N. Bjørnstad, A. M. Liebhold, and D. C. Reuman. 2017. The geography of spatial synchrony B. Blasius [ed.]. Ecol Lett **20**: 801–814. doi:10.1111/ele.12782

Watras, C. J., P. C. Hanson, T. L. Stacy, K. M. Morrison, J. Mather, Y.-H. Hu, and P. Milewski. 2011. A temperature compensation method for CDOM fluorescence sensors in freshwater: CDOM temperature compensation. Limnol. Oceanogr. Methods **9**: 296–301. doi:10.4319/lom.2011.9.296

Webster, K. E., T. K. Kratz, C. J. Bowser, J. J. Magnuson, and W. J. Rose. 1996. The influence of landscape position on lake chemical responses to drought in northern Wisconsin. Limnol. Oceanogr. **41**: 977–984. doi:10.4319/lo.1996.41.5.0977

Wilkinson, G. M., J. Walter, R. Fleck, and M. L. Pace. 2020. Beyond the trends: The need to understand multiannual dynamics in aquatic ecosystems. Limnol Oceanogr Letters **5**: 281–286. doi:10.1002/lol2.10153

Wynne, R. H., J. J. Magnuson, M. K. Clayton, T. M. Lillesand, and D. C. Rodman. 1996. Determinants of temporal coherence in the satellite-derived 1987-1994 ice breakup dates of lakes on the Laurentian Shield. Limnol. Oceanogr. **41**: 832–838. doi:10.4319/lo.1996.41.5.0832

Zarnetske, J. P., M. Bouda, B. W. Abbott, J. Saiers, and P. A. Raymond. 2018. Generality of Hydrologic Transport Limitation of Watershed Organic Carbon Flux Across Ecoregions of the United States. Geophys. Res. Lett. **45**. doi:10.1029/2018GL080005

Supplementary information for:

Synchrony dynamics of dissolved organic carbon in high-mountain streams: insights into scale-dependent processes

Lluís Gómez-Gener[1,2*], Nicola Deluigi[1], Tom Battin[1]

1 River Ecosystems Research Laboratory, Alpine and Polar Environmental Research Center (ALPOLE), Ecole Polytechnique Fédérale de Lausanne, EPFL, Switzerland

2 Centre for Research on Ecology and Forestry Applications, Universitat Autònoma de Barcelona, Campus de Bellaterra, Edifici C, 08193 Cerdanyola del Vallès, Barcelona, Spain

* E-mail: gomez.gener87@gmail.com (Corresponding author)

Table of Contents

Supplementary Figures

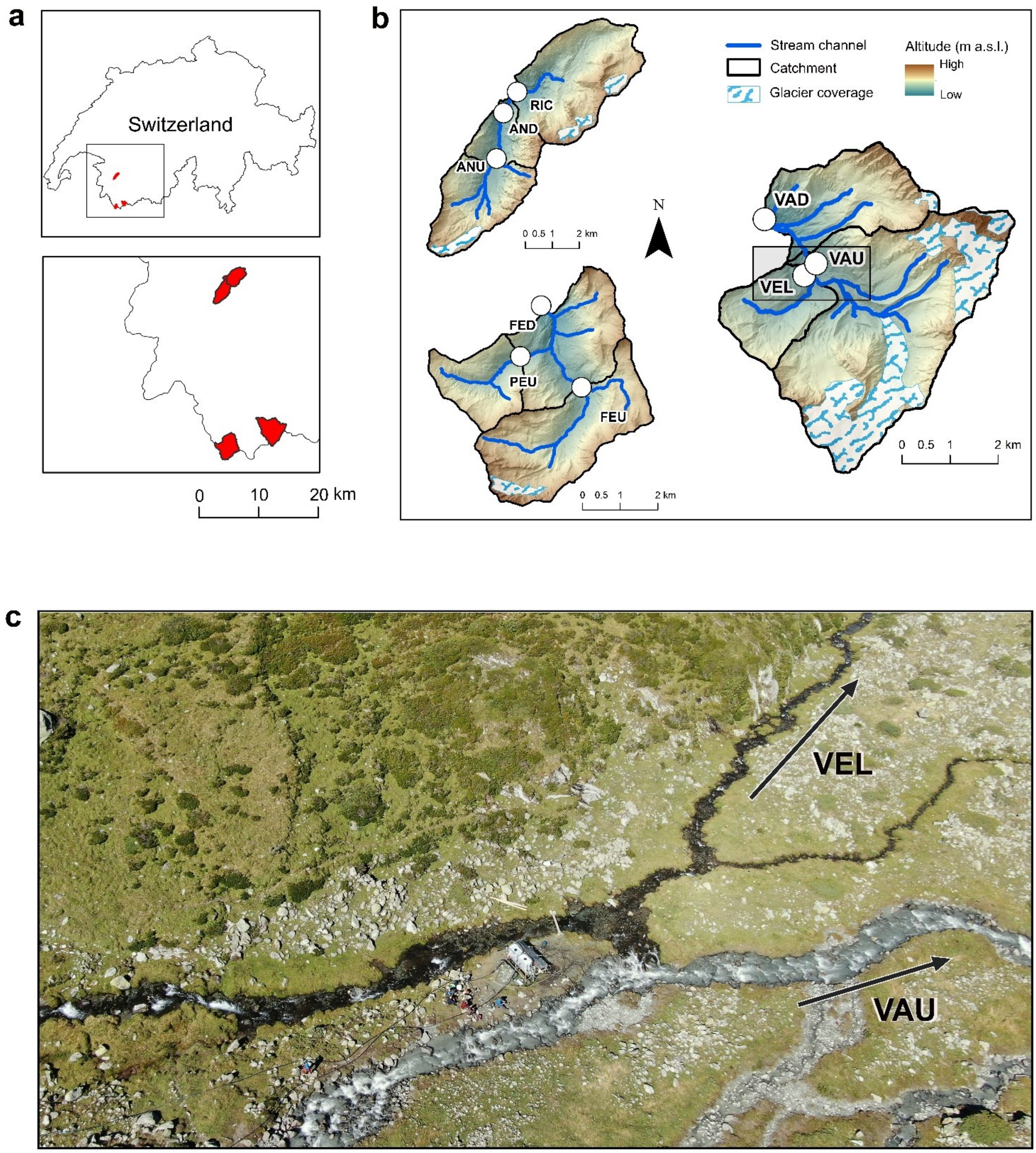

Figure S1. (a) Study region with the catchments and (**b**) stream sampling locations in the Swiss Alps. Panel (**c**) shows a visual example of two streams (VEL and VAU) representing an extreme case of similarity in their exposure to climatic factors (measured as horizontal proximity; see Table S1 and S2) but dissimilarity in their sub-catchment land cover and hydro-geomorphological attributes. VEL represents a groundwater-fed stream typical of high-mountain landscapes, while VAU represents a glacier-fed stream typical of high-mountain landscapes.

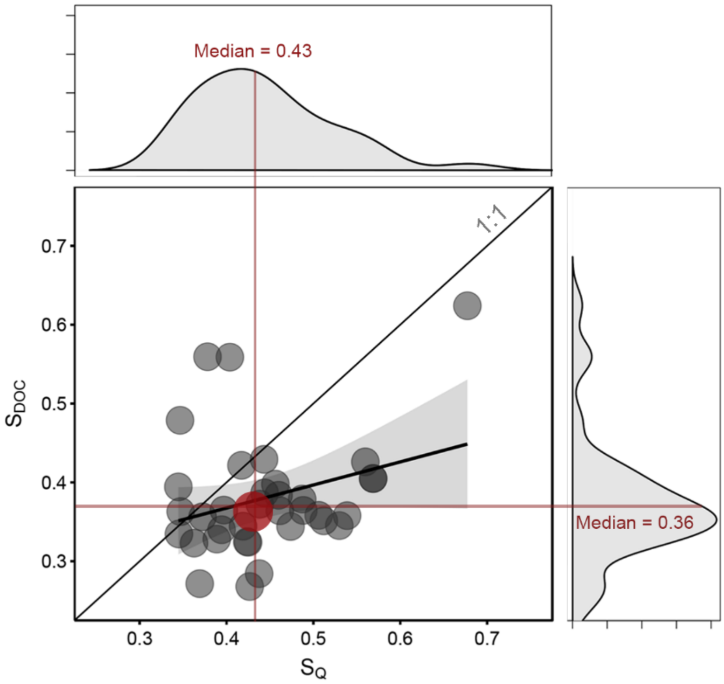

Figure S2. Relationship between timescale-aggregated S_Q and S_{DOC} for all stream pairs. The red circles indicate the intersection between medians of timescale-aggregated S_Q and S_{DOC} for the entire distribution of stream pairs.

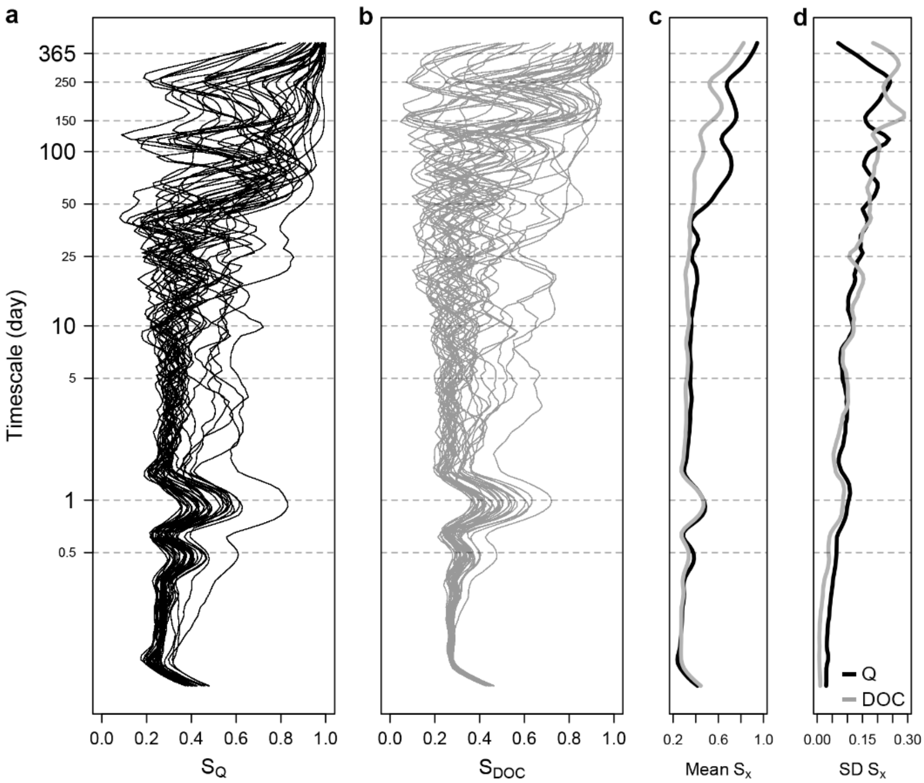

Figure S3. Temporal structure of (**a**) discharge synchrony (S_Q) and (**b**) dissolved organic carbon synchrony (S_{DOC}) for the 36 stream pairs assessed in the study. The temporal structure of the (**c**) mean and (**d**) standard deviation of S_Q (black line) and S_{DOC} (grey line) is depicted. The y-axis represents the log10-transformed period length or timescale of oscillation (in days). Horizontal dashed lines represent reference timescales.

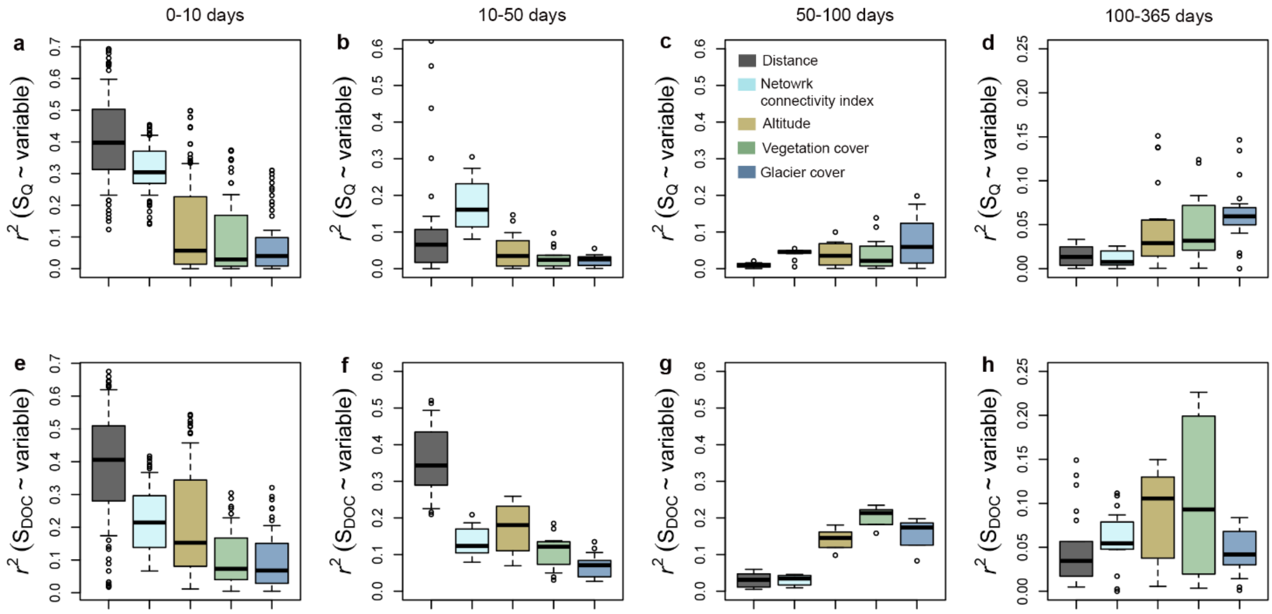

Figure S4. Boxplots summarizing the proportion of variance explained by each individual explanatory variable on S_Q and S_{DOC} at four specific timescale ranges (i.e., 1-10, 10-50, 50-100, and 100-365 days).

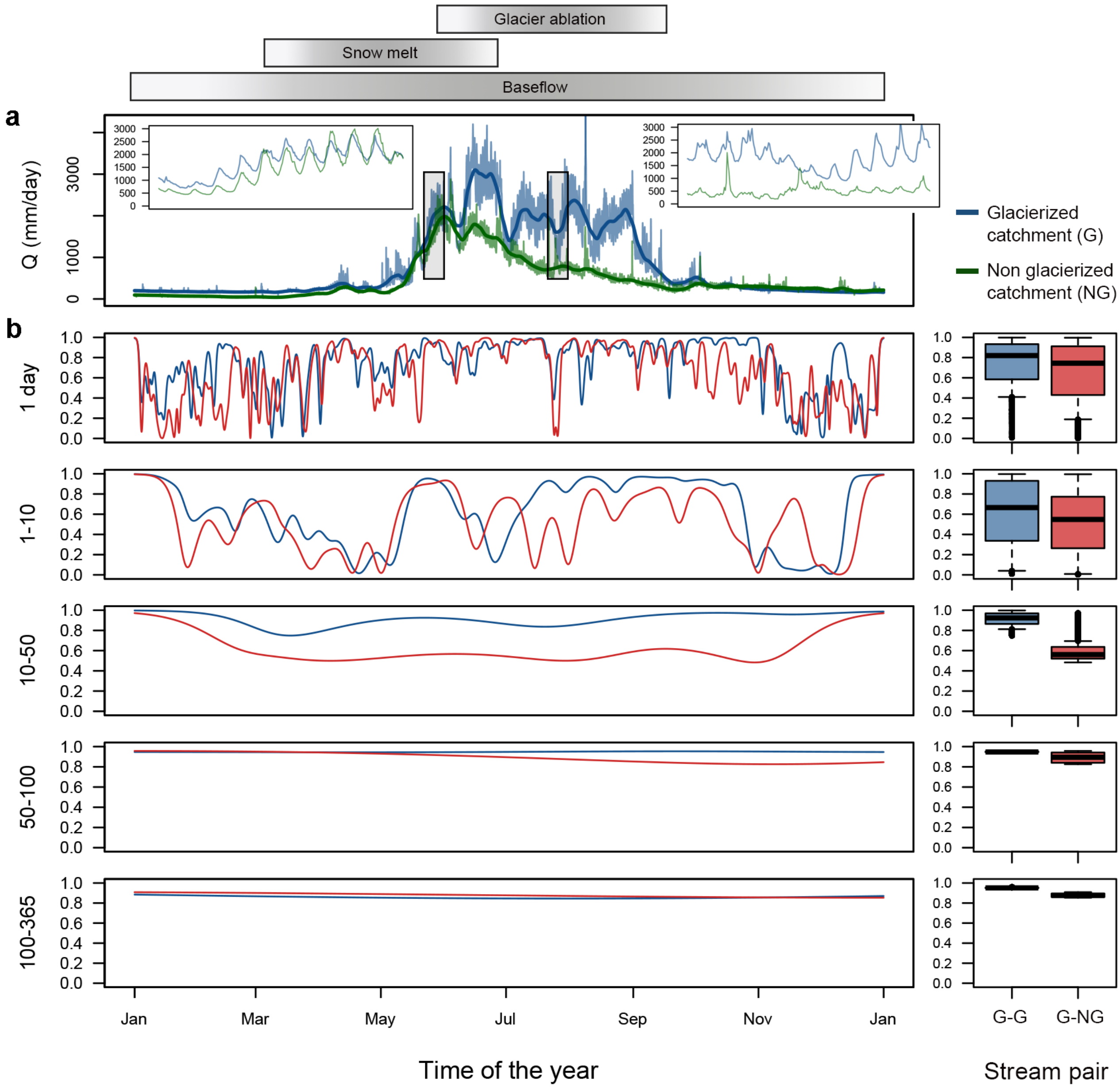

Figure S5. High-frequency time series of (**a**) dicharge (Q) and (**b**) runoff synchrony (S_Q) between two selected stream pairs across five specific timescale ranges (1, 1-10, 10-50, 50-100, and 100-365 days). The first pair (VAU and VEL) consists of two neighboring streams (Figure S1) that differ in their sub-catchment land cover and hydro-geomorphological attributes (Table S1 and S2). VAU remains under the influence of glacier ice melt dynamics (G), while VEL is a groundwater-fed stream draining a non-glacierized catchment (NG). O the other hand, the two streams in the second pair (VAU and VAD), both influenced by glacier dynamics (G), show high similarity indices in terms of exposure to climatic factors and sub-catchment attributes (Table S1 and S2) and are used as reference for the maximum expected pair S. The right panels display boxplots comparing differences in S between stream pairs (G-G vs. G-NG) at the five specific timescale ranges. Box plots show the 25th, 50th, and 75th percentiles while whiskers represent the 10th and 90th percentiles. To normalize and compare discharge from the twostreams with different catchment areas, we report specific discharge (mm day^{-1}) in panel (**a**).

Supplementary Tables

Table S1. Geographical and landscape characteristics of the nine streams in the Swiss Alps.

Stream code	Stream location		Catchment properties				
	Latitude (°)	Longitud (°)	Altitude (m a.s.l.)	Surface area (km^2)	Vegetation (%)[a]	Glacier and perpetual snow (%)[a]	Mineral surfaces (%)[a]
VAU	45.9295	7.2446	2148	18.1	21.1	33.5	45.4
VAD	45.9350	7.2269	1937	23.2	24.2	27.4	48.4
VEL	45.5568	7.1475	2161	3.1	56.7	0.0	43.3
FEU	45.8831	7.1309	1995	9.3	46.3	7.4	46.3
FED	45.9051	7.1156	1774	20.2	62.4	3.4	34.2
PEU	45.8937	7.1080	2027	4.0	70.2	0.0	29.8
ANU	46.2316	7.1020	1465	9.0	54.0	6.8	39.2
AND	46.2534	7.1096	1201	13.4	63.9	4.6	31.5
RIC	46.2535	7.1101	1200	14.3	64.2	6.4	29.4

[a] Vegetation, glaciers, and perpetual snow, and mineral surfaces cover percentages based on the CORINE Land Cover Inventory 2012. The percent vegetation cover includes mixed and coniferous forests, moors, heathlands, pastures, sparsely vegetated areas, and natural grassland land cover layers.

Table S2. Similarity index between stream pairs for the geographical and landscape characteristics of the nine streams in the Swiss Alps.

Linear distance (km)

	VAU	VAD	VEL	FEU	FED	PEU	ANU	AND	RIC
VAU									
VAD	1.03								
VEL	0.22	1.22							
FEU	10.20	9.66	10.21						
FED	10.46	9.64	10.36	2.20					
PEU	11.37	11.37	10.69	1.70	1.42				
ANU	35.25	34.57	35.53	38.32	36.29	37.56			
AND	37.13	36.64	37.37	40.63	38.62	39.91	2.46		
RIC	37.23	36.74	37.47	40.73	38.72	40.01	2.53	0.10	

Stream connectivity index

	VAU	VAD	VEL	FEU	FED	PEU	ANU	AND	RIC
VAU									
VAD	2								
VEL	0	1							
FEU	0	0	0						
FED	0	0	0	2					
PEU	0	0	0	0	1				
ANU	0	0	0	0	0	0			
AND	0	0	0	0	0	0	2		
RIC	0	0	0	0	0	0	0	0	

Mean catchment altitude (m a.s.l.)

	VAU	VAD	VEL	FEU	FED	PEU	ANU	AND	RIC
VAU									
VAD	2042.5								
VEL	2154.5	2049.0							
FEU	2071.5	1966.0	2078.0						
FED	1961.0	1855.5	1967.5	1884.5					
PEU	2087.5	1982.0	2094.0	2011.0	1900.5				
ANU	1806.5	1701.0	1813.0	1730.0	1619.5	1746.0			
AND	1674.5	1569.0	1681.0	1598.0	1487.5	1614.0	1333.0		
RIC	1674.0	1568.5	1680.5	1597.5	1487.0	1613.5	1332.5	1200.5	

Mean vegetation cover (%)

	VAU	VAD	VEL	FEU	FED	PEU	ANU	AND	RIC
VAU									
VAD	22.6								
VEL	38.9	40.5							
FEU	33.7	35.2	51.5						
FED	41.7	43.3	59.6	54.3					
PEU	45.7	47.2	63.5	58.2	66.3				
ANU	37.5	39.1	55.4	50.1	58.2	62.1			
AND	42.5	44.1	60.3	55.1	63.2	67.1	59.0		
RIC	42.7	44.2	60.5	55.2	63.3	67.2	59.1	64.1	

Mean glacier cover (%)

	VAU	VAD	VEL	FEU	FED	PEU	ANU	AND	RIC
VAU									
VAD	30.4								
VEL	16.8	13.7							
FEU	20.5	17.4	3.7						
FED	18.5	15.4	1.7	5.4					
PEU	16.8	13.7	0.0	3.7	1.7				
ANU	20.2	17.1	3.4	7.1	5.1	3.4			
AND	19.0	16.0	2.3	6.0	4.0	2.3	5.7		
RIC	19.9	16.9	3.2	6.9	4.9	3.2	6.6	5.5	

Mean mineral surface cover (%)

	VAU	VAD	VEL	FEU	FED	PEU	ANU	AND	RIC
VAU									
VAD	48.9								
VEL	41.1	42.4							
FEU	52.1	53.3	45.6						
FED	44.4	45.6	37.9	48.8					
PEU	43.2	44.5	36.7	47.7	40.0				
ANU	49.2	50.4	42.7	53.6	45.9	44.8			
AND	46.5	47.8	40.1	51.0	43.3	42.1	48.1		
RIC	45.4	46.6	38.9	49.8	42.1	41.0	46.9	44.3	

Table S3. Statistical summary of regressions between timescale aggregated S_Q (above) and S_{DOC} (below) and the set of potential explanatory variables.

S_Q ~ variable	**r^2**	**slope**	***p-value***
Distance	**0.49**	**-0.03**	**< 0.001**
Network connectivity	**0.22**	**0.060**	**< 0.001**
Altitude	0.01	0.001	0.65
Glacier cover	0.06	0.002	0.15
Vegetation cover	0.05	-0.002	0.20
S_{DOC} ~ variable			
Distance	**0.57**	**-0.05**	**< 0.001**
Network connectivity	**0.20**	**0.058**	**< 0.001**
Altitude	**0.21**	**0.001**	**< 0.001**
Glacier cover	0.06	0.003	0.15
Vegetation cover	**0.13**	**-0.003**	**0.03**

Table S4. Statistical summary of regressions between S_Q and S_{DOC} and distance between stream locations for both timescale aggregated (measured as the median coherence for all the timescales) and timescale segregated at six specific timescales or timescale bands (i.e., 1, 1-10, 10-50, 50-100, 100-365, and 365 days).

Timescale band (days)	**S_Q ~ distance**			**S_{DOC} ~ distance**		
	r^2	***slope***	***p-value***	***r^2***	***slope***	***p-value***
Aggregated	**0.49**	**-0.03**	**< 0.001**	**0.57**	**-0.05**	**< 0.001**
1	**0.52**	**-0.05**	**< 0.001**	**0.39**	**-0.03**	**< 0.001**
10-ene	**0.53**	**-0.03**	**< 0.001**	**0.58**	**-0.02**	**< 0.001**
10-50	0.18	-0.03	0.06	**0.46**	**-0.06**	**< 0.001**
50-100	-0.02	0.001	0.96	**0.12**	**-0.04**	**0.02**
100-365	-0.02	-0.01	0.55	0.03	-0.02	0.14
365	0.01	0.01	0.73	**0.14**	**-0.05**	**0.01**